

Models for Weak Wind and Momentum Problems in the Winds of Hot Stars

O. Vilhu¹ and T.R. Kallman²

¹ Dept of Physics, P.O. Box 84, FI-00014 University of Helsinki, Finland
e-mail: osmi.vilhu@gmail.com

² Lab. for High-Energy Astrophysics, NASA/GSPC, Greenbelt, Maryland, USA e-mail: timothy.r.kallman@nasa.gov

Received ; accepted

ABSTRACT

Context. Hot star winds are laboratories for 3-dimensional radiative hydrodynamics and for X-ray sources with wind accretion. In this context analytic models presented here are helpful.

Aims. The CAK-method (Castor, Abbot & Klein, 1975) has been succesful for giants and supergiants of normal OB-stars but has failed to explain the weak winds of main sequence low luminosity OB-stars ('weak wind problem'). Further, CAK has never been applied seriously to WR-stars and was considered as a mission impossible due to the 'momentum problem'. The aim is to reevaluate the analytic CAK-method, to recalculate proper force multipliers, numerically solve the wind equations for a sample of O- and Wolf Rayet (WR) -stars and to obtain their mass loss rates and wind velocities. The secondary aim is to solve the *weak wind and momentum problems* of hot star winds.

Methods. The wind in the supersonic part was modelled by photoionized plasma and radiative force (force multiplier) using the XSTAR-code (Kallman & Bautista, 2001, Stevens & Kallman, 1990). The force multiplier FM was computed as a function of the absorption parameter τ , ionizing parameter ξ , particle number density N , chemical composition and the ionizing source spectrum. The force was included in the momentum equation, and together with the mass conservation solved numerically in the supersonic part of the wind for a sample of O- and WR- stars (WN-type). The input parameters were the basic stellar parameters (mass, radius, luminosity, chemical composition). The results depend also on the boundary condition of subsonic part and the velocity law. Fitting with the β -law with fixed $\beta=0.6$ and $v_{in} = 10$ km/s approximate these and gave the mass loss rate and wind velocity as outputs. Mass clumping was introduced by the volume filling factor F_{vol} scaling ξ by F_{vol}^{-1} . Velocity clumping was approximated by the velocity filling factor $FVEL$ modifying the force multiplier (following Sundqvist et al., 2014).

Results. Force multipliers based on blackbody radiators can be used for O-stars, while cut blackbodies (flux below 230 Å cut to zero) approximate well those of WR-stars. O-stars require moderate clumping $F_{vol} = 0.13$ to match the canonical Vink-prediction (Vink et al. 2001). The low mass loss rates of main sequence late O-stars (weak wind problem) can be explained by velocity clumping ($FVEL = 0.1$). The momentum problem of WR-stars is shown to be due to wrong treatment of the input ionizing spectrum resulting in too small force multiplier. Due to heavy absorption in WR-winds the flux below 230 Å (He II ionization) is zero enhancing greatly the number of absorbing heavy element lines, and consequently the force multiplier, by eliminating the suppression by soft X-rays. The computed mass loss rates and terminal wind velocities for 40 OB-stars and 55 WR-stars (WN type) are given in Tables A1 and A2 and Figs. 10-14.

Conclusions. A possible solution for the weak wind problem of low luminosity late O-stars was quantitatively studied and explained by a small velocity filling factor $FVEL$. The momentum problem of WR-winds was solved by proper computation of the line force with correct radiator (cut to zero below 230 Å). The problem is an opacity problem of simply identifying enough lines (Gayley et al. (1995)). The present paper is the first comprehensive and self consistent treatment and numerical solutions of hot star wind equations. Starting from the basic stellar parameters (mass, radius, luminosity, chemical composition) the wind equations were solved fitting with the β -law (with fixed $\beta=0.6$) giving mass loss rate and wind velocity as results. The computed mass loss rates match well with the observed/predicted ones. The effects of free parameters β , F_{vol} and $F_{vel}=FVEL$ were quantitatively estimated. The eventual X-ray suppression on the face-on side of Cyg X-3 may act like lowering of $FVEL$, leading to decreasing of both mass loss rate and wind velocity.

Key words. Stars: early type — Stars:Wolf Rayet — Stars: mass loss — Stars: winds

1. Introduction

Hot star winds are accelerated by the radiation pressure in lines. The properties of such winds were first comprehensively explored by Castor, Abbott & Klein, 1975, hereafter CAK. This theory is based on the Sobolev approximation to compute the local line force, that is, that the line broadening is dominated by

the bulk motion of the wind, and that photons from the stellar photosphere only interact once as they escape the wind.

CAK showed that the effects of line scattering can be represented by the ratio of the opacity produced by the ensemble of lines to the electron scattering opacity and can be represented by a number, called the force multiplier, and that this quantity can be very large ($\geq 10^4$) in hot stars. The formalism developed by CAK has been succesful in describing the wind properties, i.e. wind speeds and mass loss rates, in giants and supergiants of nor-

Send offprint requests to: O. Vilhu

mal OB-stars. However, it does not provide correct predictions for the mass loss rates of main sequence low luminosity OB-stars (hereafter called the ‘weak wind problem’). Furthermore, the CAK formalism has not been applied to Wolf-Rayet (WR) stars, owing to the fact that winds from these stars appear to have more momentum than is available from the stellar radiation field (hereafter called the ‘momentum problem’). Wind models which do not rely on the Sobolev approximation have been developed in order to produce 2-D simulations (see e.g. Sundqvist et al. 2018). In these simulations density and velocity clumpings arise in a physical way.

Explanations which have been suggested for the ‘weak wind problem’ include the effects of X-rays (Marcolino et al. 2009), magnetic fields (Shenar et al. 2017) or velocity clumping (Sundqvist et al. 2014). Leakage of light associated with porosity in velocity space could lead to lowering of starlight power (line force) and consequently to lower mass loss rate. This last possibility will be studied in detail in the present paper.

Another problem with the CAK-theory has been its inability to explain the massive winds of Wolf Rayet stars. This is called the ‘momentum problem’. The name comes from the ratio of wind momentum to radiation momentum $\eta = \dot{M} v_{\infty} / (L/c)$ which is much larger than 1 for WR-stars. However, as pointed out by Gayley et al. (1995), the problem may be just due to the problem of identifying enough lines. If this is the case then the CAK force multiplier generally accepted is too small. In the present paper the force multipliers are recalculated using realistic radiation spectra for WR-stars and found that this is the case (at least for the WN subclass of hottest WR stars).

In the present paper we use the extensive XSTAR code and data base (Kallman & Bautista, 2000; Stevens & Kallman, 1990) to compute force multipliers. The wind equations (mass conservation and momentum balance) for a sample of O- and WR-stars will be solved in one dimension. Inputs include basic stellar parameters: mass, radius, luminosity and chemical composition. The wind equations are integrated, and the resulting velocity law is fitted with an analytic form which is similar to the formula derived by CAK, and which is in widespread use for describing hot star winds. The output solutions are the two quantities describing the wind global properties: mass loss rate and terminal velocity. We also use the analytic modification of the line force developed by Sundqvist et al. (2014) to include velocity clumping in the formalism. Density clumping is included by using a volume filling factor modifying the ionization parameter ξ .

We discuss the derived mass loss rates and terminal velocities in the context of other estimates and examine the effects of clumping in density and velocity.

2. The Line Force (Force multiplier)

2.1. Method of computation

The force multiplier FM was computed following the method described by CAK. An important difference is that CAK (and other compilations, eg. Gayley et al. 1995) assume that the ionization and excitation in the wind is given by a Saha-Boltzmann distribution modified by an analytic dilution factor applied to all elements. We compute the ionization distribution in the wind by balancing the ionization and recombination due to the stellar radiation field. We also employ the Boltzmann distribution to determine the populations of excited levels. The radiation field is computed using a single-stream integration outward from the stellar photosphere. In this way we calculate the line force appropriate to any spectral form of the photospheric spectrum and at

any layer in the wind. This permits us to integrate wind equations from the surface to infinity in a self-consistent manner since the upwards force is known.

The ionization balance and outward transfer of photospheric radiation are calculated using the XSTAR photoionization code (Stevens & Kallman, 1990; Kallman & Bautista, 2000; Kallman, 2018). The ion fractions at each spatial position in the wind are used to calculate the force multiplier FM by summing the CAK line force expression over an ensemble of lines. The list of lines is taken from Kurucz (<http://kurucz.harvard.edu/linelists.html>) and permits us to use local wind parameters. The line list is more extensive than in the original CAK-work. It is assumed that the wind is spherically symmetric around the donor star (the ionizing source).

XSTAR calculates the ionization balance for all the elements with atomic number $Z \leq 30$ together with the radiative equilibrium temperature. It calculates full non-LTE level populations for all the ions of these elements. It includes a fairly complete treatment of the level structure of each ion, i.e. more than ~ 50 levels per ion, and up to several hundred levels for some ions. Many relevant processes affecting level populations are included, i.e. radiative decays, electron impact excitation and ionization, photoionization, and Auger decays. All processes include their inverses such that they obey detailed balance relations and populations approach LTE under the appropriate circumstances. The electron kinetic temperature is calculated by imposing a balance between heating from fast photoelectrons and Compton scattering with radiative cooling.

Key simplifications employed by XSTAR are with regard to the radiative transfer solution. Escape of line radiation is treated using an escape probability formalism, and this affects the temperature via the net radiative cooling. Transfer of the ionizing continuum is treated using a single-stream integration of the equation of transfer, including opacities and emissivities calculated from the local level populations etc. Thus there is no allowance for the inward propagation of diffusely emitted radiation. This last approximation is likely to be most important for the results presented here, since strong winds can have large optical depths in the ionizing continua of hydrogen and He II. It would be desirable to verify our current results using a transfer solution which does not have this limitation. Limitations of the escape probability assumption for line escape have been pointed out by eg. Hubeny (2001). However, for hot star winds the strong velocity gradient reduces most line optical depths to $\sim a$ few at most, and so the lines are effectively thin and the radiative cooling is not strongly affected.

The force multiplier $FM(t, \xi, N)$ is a 3-dimensional function of the absorption parameter t , ionizing parameter ξ and particle number density N :

$$t = \sigma_e v_{th} \rho (dv/dr)^{-1} \quad (1)$$

$$\xi = \frac{L_{ly}}{N r^2} \quad (2)$$

Here L_{ly} is the incident luminosity below the Hydrogen ionization limit 912 \AA , σ_e is the electron scattering coefficient, ρ and N the gas and particle number density, respectively, v is the outward wind velocity, r the radial distance from the ionizing source and v_{th} is the gas thermal velocity (typically $\sim 10 \text{ km/s}$). The force multiplier was computed assuming a point source radiator. When applied to stars, the dilution factor r^{-2} in eq.2 should be replaced by the finite disk one (eq.15). The chemical abundances of the wind, as well as the ionizing source spectrum, can

be specified as input data. The method is in principle the same as in the classical work of CAK. However, in the present work ξ and t are explicitly included and computed locally in the wind.

The force multiplier depends on t and on the cross section for line absorption:

$$FM(t, \xi) = \sum_{lines} \frac{\Delta \nu_D F_\nu}{F} \frac{1}{t} (1 - e^{-\eta t}) \quad (3)$$

where $\Delta \nu_D$ is the thermal Doppler width of the line, F is the total flux in the continuum, F_ν is the monochromatic flux at the line energy, and

$$\eta = \kappa_{line} / \sigma_e \quad (4)$$

$$\kappa_{line} = \frac{\pi e^2}{m_e c} g_L f \frac{N_L / g_L - N_U / g_U}{\rho \Delta \nu_D} \quad (5)$$

where N_L and N_U are the lower and upper level populations, g_i are the statistical weights, and f is the oscillator strength. Our code (`xstarfmult.f`) uses the ion fractions calculated as described above to sum over lines and calculate $FM(t, \xi)$. Ground state level populations are taken directly from XSTAR; excited level populations are calculated assuming a Boltzmann (LTE) distribution. This is necessitated by the use of the Kurucz line list, which does not include collisional rates or other level-specific quantities which would allow a full non-LTE calculation of populations which can be used for the calculation of κ_{line} . Most previous calculations of the CAK force multipliers have employed the LTE assumption for excited levels as well (eg. CAK, Abbott 1982, Gayley 1995).

An extensive set of $FM(t, \xi, N)$ -grids were computed with varying chemical composition, ionizing source spectrum and particle number density N . Dependence on the gas density is primarily through the ionization parameter ξ . In our computations gas thermal velocity of Hydrogen atoms was used. As noted by CAK, Abbott (1982) and Stevens & Kallman (1990), the force multiplier is independent of thermal velocity if the same value is used for both FM -tables and t -parameter calculations.

Examples of the force multiplier are shown in Fig.1 computed with solar abundances (Asplund et al. 2009) and $N=10^{12} \text{ cm}^{-3}$. Comparison with the widely used CAK-formula $FM = 1/30 \times t^{-0.8}$ shows agreement at high ionization parameter values for 33 000 K blackbody. The CAK calculations used a smaller list of lines, which is the likely explanation for the fact that the dashed line generally lies below the current calculations. The effects of other parameters are illustrated in Fig.2. The ionizing source spectra used in Figs 1 and 2 are shown in Fig.3.

2.2. Effect of chemical abundances

The difference between solar abundances (by mass X (Hydrogen) = 0.71, Y (Helium) = 0.27, Z (Heavy elements) = 0.015) and Hydrogen deficient WN-abundances ($X = 0.085$, $Y = 0.9$, $Z = 0.015$) is moderately small if for individual heavy elements the same solar abundances are used. This is demonstrated in Fig.2 for the Set 1 of radiators, the dotted lines showing force multipliers for Hydrogen deficient abundances. The effect of equilibrium CNO-abundances in WN stars is negligible. Fig.2 was computed with solar abundances but the dashed line in the set 3 shows the line force for equilibrium CNO-abundances (hardly visible). The effect is small, only at very low t -values ($\log(t)$ less than -5) the effect is meaningful.

At small t -values the force multiplier is proportional to Z , at large t -values the Z -dependence is weaker.

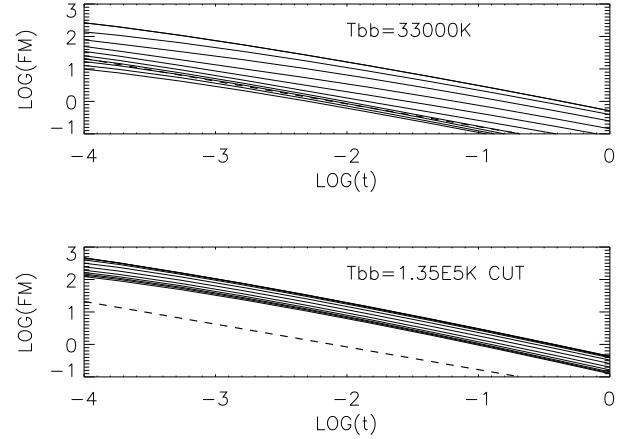


Fig. 1. Examples of force multipliers. Solar abundances were used and the ionizing source is a blackbody with $T = 33\,000\text{ K}$ (O-stars, upper plot) and a cut blackbody with $T=135\,000\text{ K}$ (WR-stars, lower plot, see Fig.3). The logarithm of the ionizing parameter ξ range from 0 (uppermost curve) to 4.5 (lowest). The CAK-formula $FM = 1/30 \times t^{-0.8}$ is shown by the dashed line. A density value of $N = 10^{12} \text{ cm}^{-3}$ was used in this calculation.

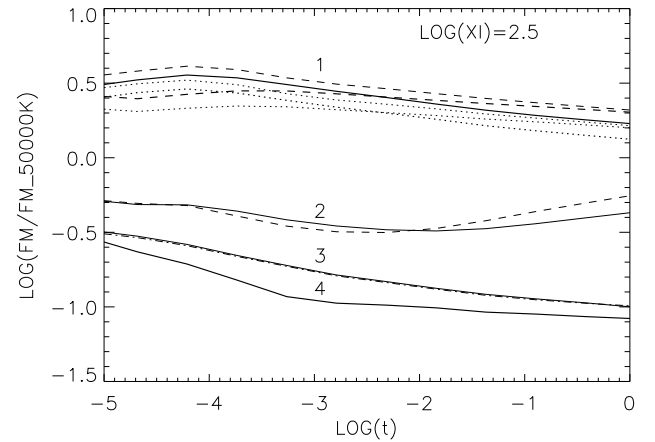


Fig. 2. Force Multipliers relative to 50 000 K blackbody at $\log(\xi) = 2.5$ using solar abundances. The curves are grouped and labeled with the ionizing source type as follows (see Fig.3) : 1: blackbody with $T = 135\,000\text{ K}$ but cut to zero below 230 Å (solid line), Potsdam model WNE16-20 (dashed line) and the mean computed WR-model (the present study) at $\delta(r/R_{star}) = 0.01$ above the surface (dashed line). 2: blackbody with $T = 33\,000\text{ K}$ (solid line) and Potsdam model OB33-36 (dashed line). 3: blackbody with $T = 100\,000\text{ K}$ (solid line) and the same blackbody but with WN-abundances (dashed line, hardly visible). 4: blackbody with $T = 135\,000\text{ K}$. The dotted lines show force multipliers for the Set 1 with Hydrogen deficient abundances (see the text).

2.3. Effect of radiator spectral shape

The spectral shape below 912 Å , particularly below the Helium 2nd ionization limit 230 Å , is crucial. This can be seen in Fig.2 by comparing the curves drawn by solid lines and labeled by '4' (blackbody $T = 135\,000\text{ K}$) and by '1' (the same blackbody $T = 135\,000\text{ K}$ but cut to zero below 230 Å). The cut part represents soft X-rays which heavily suppress the force multiplier as found already by Stevens & Kallmann (1990). Fig.2 shows quantitatively how the force multiplier of cut $135\,000\text{ K}$ blackbody is

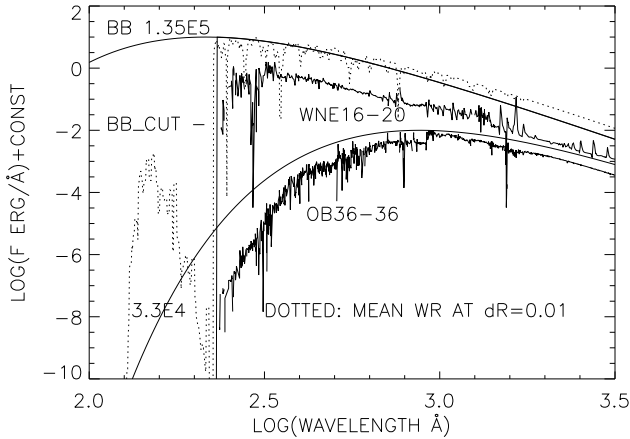


Fig. 3. The ionizing source spectra used for force multipliers in Fig. 2. blackbodies with $T = 135\,000\text{ K}$ (cut and non-cut) and $T = 33\,000\text{ K}$ are shown by continuous solid lines. The Potsdam WR-model WNE16-20 and OB-model OB33-36 show strong absorptions (solid lines). The dotted line is the mean spectrum of WR-stars at 1 percent (in stellar radius) above the surface (the present study). The curves can be shifted vertically.

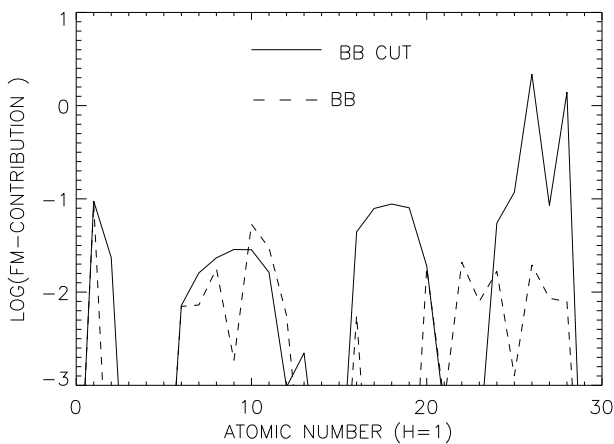


Fig. 4. Contributions to the force multiplier (FM) as a function of the element atomic number (26 for Fe). $135\,000\text{ K}$ blackbody (dashed line) and cut blackbody with the same temperature (solid line) were used as radiators and the force multiplier was calculated at $\log(\xi) = 2.5$ and $\log(t) = -1.84$ (see Fig. 2). Note the logarithmic scale of y-axis.

over 10 times larger than that of a pure blackbody. Figures 4 and 5 show this effect as a function of element atomic number and wavelength. The soft X-ray suppression clearly vanishes when flux below 230 Å is absorbed away, making the iron group elements contribution larger.

The effect of blackbody temperature is moderately large. Force multipliers of blackbodies between $25\,000\text{ K}$ - $50\,000\text{ K}$ do not differ from those using corresponding Kurucz-models (Kurucz, 1979) for an average O-star. However, force multipliers computed with $50\,000\text{ K}$ and $25\,000\text{ K}$ Kurucz models are somewhat smaller and larger, respectively, than those with corresponding blackbodies.

When integrating the equations of motion the absorption was included. This changed the spectral form and luminosity below 912 Å , the limit below which the ionization parameter ξ is com-

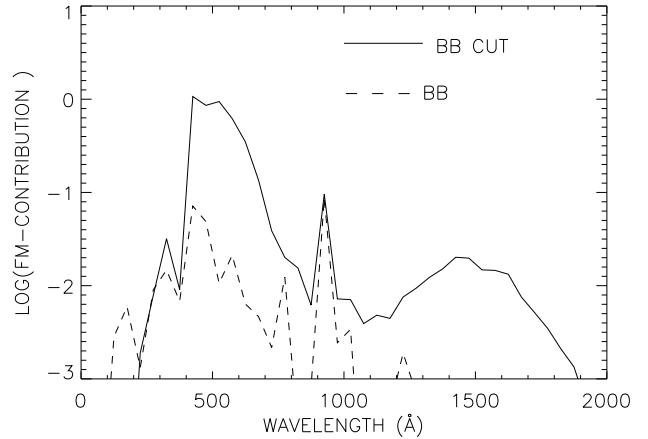


Fig. 5. The same as in Fig. 4 but contributions to the force multiplier inside 50 Å wide bands are shown as a function of wavelength.

puted. WR-stars with massive winds develop rapidly, close to the surface, a spectral form where fluxes at short wavelengths (in particular below 230 Å , HeII ionization edge) are significantly reduced. Already at a few percent (of stellar radius) above the surface, the flux below 230 Å drops by a factor over 10. At the same time the overall reduction below 912 Å is just by a factor of 2 or less. This is due to the large increase in absorption below 230 Å . For O-stars, with smaller mass loss rates, this effect is negligible. Hence, in Fig. 2 the $33\,000\text{ K}$ blackbody and the Potsdam model of the same temperature OB33-36 (Hainich et al. 2019, $T = T_{\text{star}} = 33\,000\text{ K}$) are very similar.

The mean WR-spectrum at $\delta(r/R_{\text{star}}) = 0.01$ and the force multiplier based on it are included in Figures 2 and 3. The result is almost the same for the Potsdam model WNE16-20 (Todt et al. 2015, $T = 141\,300\text{ K}$). Hence, the force multiplier based on cut blackbody represents well the force multiplier based on realistic WR-spectrum (see Ch. 3.3).

The momentum/opacity problem is illustrated in Figs. 4 and 5 using $135\,000\text{ K}$ blackbody as the radiator (both pure BB and cut BB, spectrum cut to zero below 230 Å). The cut blackbody gives over 10 times larger contribution to the force multiplier than the pure BB, compatible with Fig. 2.

Based on the discussion above a grid of force multiplier tables was computed for 10 blackbodies. Five blackbodies between $20\,000\text{ K}$ - $50\,000\text{ K}$ were used for O-stars and five blackbodies between $100\,000\text{ K}$ - $150\,000\text{ K}$ were cut below 230 Å (fluxes set to zero) and used for WR-stars. For an individual star, with a specific temperature, the force multiplier was interpolated from the grid.

2.4. Dependence on particle density

The particle number density N is involved explicitly in FM (resulting in a rather weak dependence) and in the ionization parameter ξ . Fig. 6 shows the N - dependence for a typical WN-star ($135\,000\text{ K}$ cut blackbody) and O-star ($33\,000\text{ K}$ blackbody) as a function of N and ξ at fixed $\log(t) = -2.8$. The δ -parameter shown characterises the density-dependence of force multiplier and is defined as the derivative

$$\delta = d[\log(FM)]/d[\log(N)] \quad (6)$$

Results are shown for different values of ξ and N at $\log(t) = -2.8$. The value $\delta = 0.11$, found by Abbott (1982) using Mihalas and

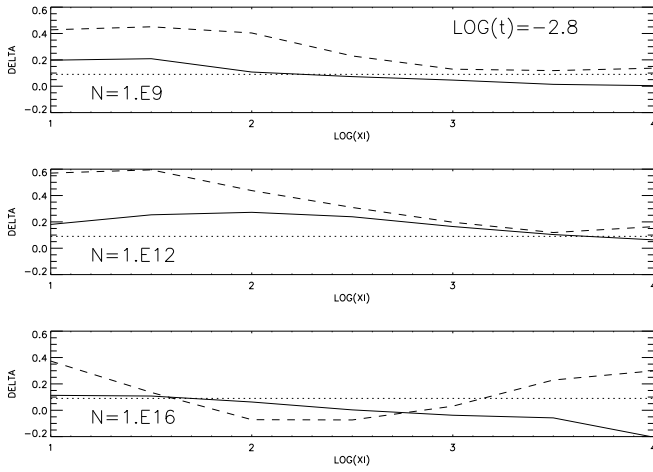


Fig. 6. The δ -parameter as a function of ionization parameter ξ for 135 000 K cut blackbody (WR stars, solid) and 33000 K blackbody (O-stars, dash) at three N -values marked (cm^{-3}). The absorption parameter is fixed at $\log(t) = -2.8$. The dotted lines show $\delta = 0.11$.

Kurucz atmospheres between effective temperatures 20 000 K - 60 000 K, is shown by horizontal dotted lines.

3. The Numerical Method

3.1. Wind Flow Equations

Only the supersonic part of the wind flow was considered (above $\delta(r/R_{\text{star}}) = 0.01$). The two equations which determine the flow are *mass conservation*

$$\dot{M} = \dot{M}_{\text{dot}} = 4\pi r^2 \rho v \quad (7)$$

and *momentum balance* (neglecting gas pressure)

$$v dv/dr = GM/r^2 [\Gamma_e(1 + g_{\text{line}}) - 1] \quad (8)$$

$$g_{\text{line}} = FM(r)F_d(r)F_{\text{vel}}^{2/3} \quad (9)$$

$$\Gamma_e = \sigma_e L / (4\pi GMc). \quad (10)$$

t , ξ and N can be computed locally, hence, $FM = FM(r)$. The momentum equation was derived by Sundqvist et al (2014) to account for velocity-clumping in the CAK-formalism. To separate better from F_{vol} we shall frequently use F_{VEL} instead of F_{vel} .

The force multiplier FM , computed in Ch.2, is multiplied by two terms reducing the upwards force: finite disc correction factor $F_d(r)$ and the normalised velocity filling factor F_{vel} (Venetian blind effect). According to Sundqvist et al. (2014) this modified line force is implemented also into the hydrodynamics code VH-1 (developed by J.Blondin and collaborators). F_{vel} is defined as

$$F_{\text{vel}} = \delta v / (\delta v + \Delta v) \quad (11)$$

δv is the velocity span inside a clump and Δv is the velocity separation between two individual clumps. In this treatment statistical averages are used. The exponent $2/3$ in $F_{\text{vel}}^{2/3}$ is the α -parameter of CAK-formalism, the slope of line strength distribution function. The value of the finite disc correction factor $F_d(r)$ is around 0.7 at stellar surface and rises to 1 at $r/R_{\text{star}} = 1.5$ and remains constant thereafter.

3.2. Solution of Wind Equations

The wind equations were integrated numerically using the IDL software, resulting in velocity stratification $v(r)$ which was compared with the widely used model

$$v_{\text{model}} = v_{\text{inf}}(1 - B/x)^\beta \quad (12)$$

$$B = 1 - (v_{\text{in}}/v_{\text{inf}})^{1/\beta} \quad (13)$$

$$x = r/R_{\text{star}}. \quad (14)$$

The integrations were started above the subsonic region at $x = 1.01$ and ended at $x = 10$, using 1000 grid points with $\delta x = 0.01$. The subsonic part of the wind enters only via the boundary condition $v_{\text{in}} = 10$ km/s in eq 13. This will be discussed in Ch. 3.3 in context with the Potsdam-model WNE 16-20. For each star M, R, L and chemical composition were used as input-values. The β -parameter was fixed to 0.6. The effect of this choice will be discussed in Ch.6. The resulting $v(x)$ was then compared with the model $v_{\text{model}}(x)$. The unknown free parameters mass loss rate \dot{M}_{dot} and v_{inf} were iterated using the IDL-procedure `mpcurvefit.pro` (written by Craig Markward), to get $(v(x) - v_{\text{model}}(x))/v_{\text{model}}(x)$ to approach zero at each x .

The procedure `mpcurvefit.pro` performs Levenberg-Marquard least squares fit, no weighting was used. The χ^2 -value (`chi2` in Tables A1 and A2) gives the goodness of fitting between the computed velocity-stratification and the velocity law (DOF=998). The formal 1-sigma errors of each parameter were computed from the covariance matrix. For this reason, these errors may not represent the true parameter uncertainties. For example, the small errors for computed \dot{M}_{dot} -values in Table A2 may be underestimated.

The effect of wind clumping was introduced by multiplying the number density N in the ionizing parameter ξ by the factor $1/F_{\text{vol}}$ where F_{vol} is the clump *volume filling factor*. The force multipliers were originally computed using point-like radiation sources with the *dilution factor* r^{-2} . However, in finite disk case in stellar atmospheres this dilution factor should be replaced by $W(r)$ given by Mewe and Schrijver (1978) and used by Vink (2000):

$$W(r) = 0.5[1 - \sqrt{1 - (R_{\text{star}}/r)^2}]. \quad (15)$$

Hence, the local ionization parameter in the wind was computed from

$$\xi(r) = L_{\text{ly}} W F_{\text{vol}} / (N_{\text{wind}} R_{\text{star}}^2). \quad (16)$$

Here N_{wind} is the number density computed from mass conservation of the wind (eq.7). This is a good assumption if the interclump space is empty and all mass is in the clumps.

3.3. Comparison with the Potsdam WR-model WNE 16-20.

Justification for the use of cut black body.

The wind equations were solved in the supersonic part of the wind (above $r/R_{\text{star}} = 1.01$) and assuming $v_{\text{in}} = 10$ km/s as the boundary condition (eq.13). Here these approximations are compared with the Potsdam model WNE 16-20 (Todt et al. 2015, <http://www.astro.physik-uni-potsdam.de/wrh/POWR/WNE/16-20>). The model parameters are: $T = 141\,300$ K, $M = 12.02$, $R = 0.748$, $\log(L) = 5.3$, $\log(\dot{M}_{\text{dot}}) = -4.83$, $v_{\text{inf}} = 1600$ km/s, $\beta = 1.0$. In the Potsdam NLTE modeling the β -law was applied above the quasi-hydrostatic region. The Potsdam data base gives model

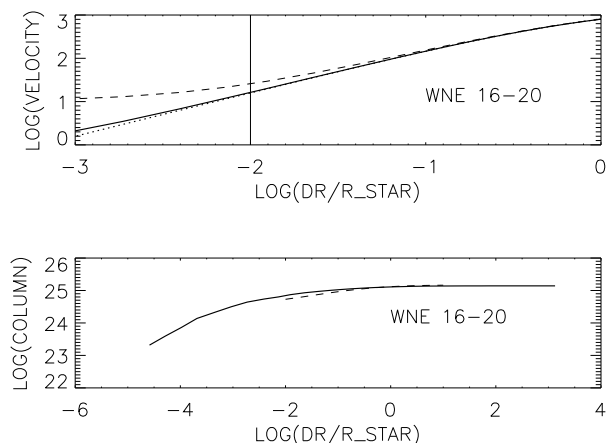


Fig. 7. Upper plot: Logarithm of wind velocity (km/s) vs logarithm of height above stellar surface ($r/R_{\text{star}}-1$) for the Potsdam WR-model WNE 16-20 (solid line). The dotted line shows the Potsdam model above the subsonic region. The dashed line is the model from the present study. The vertical line marks the height above which the wind equations were applied. Lower plot: Logarithm of the accumulated column density vs logarithm of height for Potsdam model WNE 16-20 (solid line). The dashed line shows the model from the present study.

stratifications and the outcoming spectrum. These are used here and compared with the methods of the present paper.

The numerical method of Ch.3 explained above was applied to the WNE 16-20 parameter values keeping them constant without the iteration loop. The wind velocity stratification is shown in Fig.7 (upper plot, dashed line). The lower plot shows the accumulated column density. The agreement above $r/R_{\text{star}}=1.01$ (the vertical line in the upper plot), where our flow equations were applied, is good. The present paper approximates the subsonic region by the boundary condition $v_{\text{in}} = 10$ km/s and $\beta = 0.6$. Thermal and sound velocities are around this value. This enters into our treatment via the column density estimate below $r/R_{\text{star}}=1.01$ ($3\text{E}24 \text{ cm}^{-2}$) and the β -law. For the sample of Table A2 the rise of velocity is steeper, at $r/R_{\text{star}}=1.01$ around 100 km/s. Hence, their treatment is well above the subsonic region.

Fig.8 shows the radiator fluxes smoothed by 10 \AA boxcar for WNE 16-20 of the present treatment at $r/R_{\text{star}}-1 = 0.01$ (heavy solid line) and $r/R_{\text{star}}-1 = 10$ (dashed line) and compared with the Potsdam data base emergent flux (dotted line). The 141.3 kK black body (the initial helium-star spectrum) is shown by the thin solid line. The radiation spectrum is cut below 230 \AA by 5 orders of magnitude already at the base of the supersonic region where the present treatment starts. Hence, the use of cut black bodies for computation of line force of WR-stars is justified. The removal of soft X-rays enhances the number of absorbers and consequently the line force. This is crucial for the wind acceleration in the supersonic region of Wolf Rayet stars..

4. Stellar data

The O-star sample consisted of 20 stars from Howarth & Prinja (1989, every 10th star from their list), 15 stars (models) from Kricka and Kubat (2017) and 5 low luminosity stars from Marcolino et al. (2009). The Wolf Rayet sample consisted of 29 Nitrogen type (WN) stars from Nugis & Lamers (2000), 9 hottest (T_{eff} over 80 000K) WNE-stars from Hamann et al. (2006) and 16 hottest WNE-stars (in LMC) from Hainich et al. (2014). The

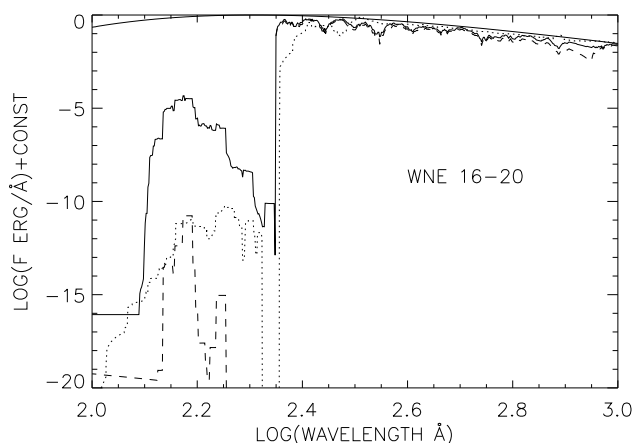


Fig. 8. Outward fluxes for the model WNE 16-20 smoothed by 10 \AA boxcar. The dotted line shows the Potsdam data base emergent model (outside the wind). The present study gives the fluxes at $r/R_{\text{star}}-1 = 0.01$ (solid line) and at $r/R_{\text{star}} = 10$ (dashed line). The broad smooth spectrum (thin solid line) is 141.3 kK blackbody used at $r/R_{\text{star}} = 1$ in the present study.

Wolf-Rayet companion of the X-ray binary Cygnus X-3 (WN-type) was added from Vilhu et al. (2009).

The data used were the basic stellar parameters: mass M , radius R , luminosity L and chemical composition. These are given in Tables A1 and A2 for the program stars with the computed values of \dot{M}_{dot} and v_{inf} (see Ch.5). The stars are shown in Fig. 7, a sort of HR-diagram.

Since only basic parameters (M , R , L , composition) were used as inputs for wind equations one might have used any grid of these parameters (e.g. from stellar evolutionary calculations). However, the above data were chosen because, besides the basic parameters, also observed and/or predicted mass loss rates and velocities were given in quoted papers, permitting comparisons.

For O-stars solar abundances (Asplund et al. 2009) were used (by mass $X = 0.71$, $Y = 0.27$, $Z = 0.015$) while for Galactic WR/WN-stars Hydrogen deficient abundances were adopted as a mean value from Nugis & Lamers (2000) ($X = 0.085$, $Y = 0.9$ and $Z = 0.015$). As found in Ch. 2.2 the use of these abundances result in rather similar force multipliers but have some influence on gas molecular weight and σ_e . For O-stars $\sigma_e = 0.33$ while for WR-stars $\sigma_e = 0.22$. For LMC-stars smaller $Z = 0.006$ was adopted (Hainich et al. 2018) lowering the force multiplier respectively.

5. Results. Computed mass loss rates.

5.1. O-stars and the weak wind problem

For the O-stars (see Ch.4 and Table A1) the wind equations were solved using Asplund (2009) solar abundances with heavy metal mass fraction $Z = 0.015$. The input parameters were masses, radii and luminosities. The β -exponent in eq. 12 was fixed to 0.6. The solution was the mass loss rate \dot{M}_{dot} and wind velocity at infinity v_{inf} . The mass loss rates and wind velocities from the references of Table A1 were used as starting points for iterations. $F_{\text{VEL}} (F_{\text{vel}})$ in eq. 9 was set to 1. Typically less than 10 iterations were needed to achieve chisquares less than 1 (DOF=998).

The results are shown in Fig. 10 where the canonical Vink-prediction (Vink 2001) is shown by the solid line. This prediction requires small volume filling factor $F_{\text{vol}} = 0.13$. With unity

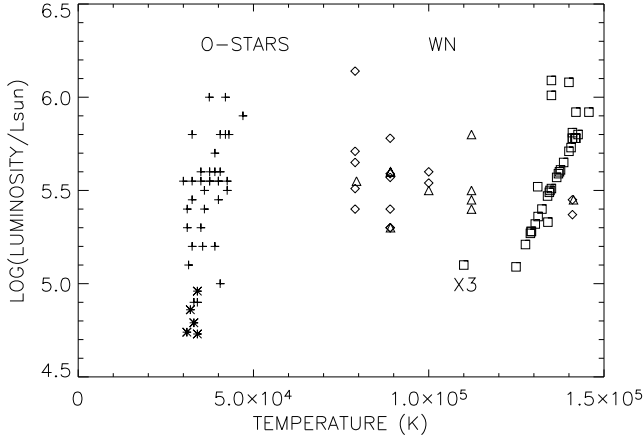


Fig. 9. Effective temperature - luminosity diagram of the program stars. O- and WR-stars are well separated in temperature. Cyg X-3 is marked by 'X3'. Meaning of symbols (see Tables A1 and A2 reference numbers): plus: 1 and 2; star: 3; square: 4 and 7; triangle: 5; diamond: 6

filling factor the results in Fig. 10 should be shifted down approximately by the amount of the stick shown in the figure (marked by F_{vol}).

In late main sequence O-stars the observed mass loss rates are much lower than predicted, contrary to giants and supergiants with higher luminosity. This is a manifestation of the 'weak wind problem'. Leakage of light associated with porosity in velocity space could lead to lowering of starlight power and consequently to lower mass loss rate. This will be the case particularly for small clump spans (eq. 18). To test this idea, small values of $FVEL = 0.1$ were applied to the main sequence low luminosity stars of Marcolino et al. (2009). With this value, the wind solutions matched well with the observations (see Fig. 10) and can in principle solve the weak wind problem. This raises the question of the physical reason behind this porosity in velocity space: why do main sequence dwarfs differ from giants and supergiants in this respect?

For low luminosity stars the mass loss rate depends on $FVEL$ as $\log(M_{dot}) = \text{const} + 1.5 \times \log(FVEL)$. For both our wind solutions and Vink-predictions the luminosity dependence of mass loss rate is steep: $\log(M_{dot}) = \text{const} + 1.7 \times \log(L)$. For Wolf Rayet stars the slope is smaller (1.2, see next Chapter). Table A1 gives the results for O-stars with $F_{vol} = 0.13$ and $FVEL=1$ except for main sequence Marcolino et al stars for which $FVEL=0.1$ was used.

5.2. WR-stars and the momentum problem.

The CAK-theory has been unable to explain the massive wind of WR-stars and this is called a 'momentum problem'. This name comes from the ratio of wind momentum to radiation momentum $\eta = M_{dot} v_{inf} / (L/c)$ which is much larger than 1 for WR-stars. However, as pointed by Gayley et al. (1995), the problem may be an opacity problem of simply identifying enough lines. We recomputed the force multipliers in Chapter 2 and found that, indeed, for realistic WR-spectra the line force is much stronger than predicted by CAK.

In Chapter 2 it was demonstrated that a cut blackbody suits well as the radiator of WR stars and was used when solving the wind equations. Fig.2 shows quantitatively how the force multiplier of cut 135 000 K blackbody is over 10 times larger than

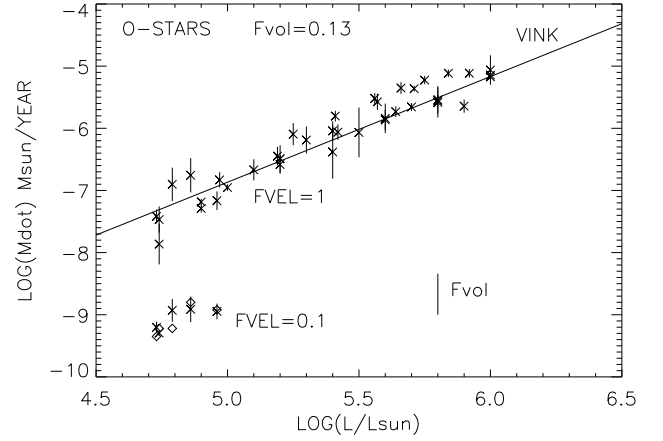


Fig. 10. Mass loss rate vs Luminosity for galactic O-stars (logarithmic scales, Table A1). Solutions of wind equations for 20 stars from Howarth and Prinja (1989), 15 models from Krticka and Kubat (2017) and 5 low luminosity stars from Marcolino et al. (2009) are shown with crosses with error bars. Asplund et al. (2009) solar abundances were used with $Z=0.015$. The clump volume filling factor $F_{vol} = 0.13$. For the Marcolino's low luminosity stars solutions with the velocity filling factor $FVEL=0.1$ are included. The Vink-prediction line (Vink et al. 2001) is added as the solid line. The diamonds show Marcolino's observations. The vertical stick marked by F_{vol} shows the upwards effect when changing the volume filling factor from 1 to 0.1.

that of a pure blackbody. Figs 4 and 5 show this as a function of element atomic number and wavelength, respectively. The soft X-ray suppression clearly vanishes when flux below 230 Å is absorbed away.

As in the case of O-stars we need only the masses, radii, luminosities and chemical composition (plus the form of velocity-law, β -law with fixed β) to solve the wind equations and obtain mass loss rates and wind velocities. For Galactic targets Asplund et al. (2009) abundances with $Z = 0.015$ were used while for the LMC-stars $Z = 0.006$ was adopted (Hainich et al. 2015). The results are shown in Fig.11 (Milky Way stars) and Fig.12 (LMC-stars). The results of all WN stars are given in Table A2 ($F_{vol} = FVEL=1$). Around 10 iterations were needed to achieve chisquares less than 5 (DOF=998).

In Figs 11 and 12 the Hainich-prescriptions (Hainich et al. 2014) are shown by dashed lines for two heavy element mass fractions ($Z = 0.006$ and 0.015). Mass loss predictions ('observations') are shown by triangles and diamonds. In Fig.11 the solid line is a linear fit to the Nugis and Lamers data. The luminosity dependence is less steep than for O-stars: $\log(M_{dot}) = \text{const} + 1.2 \times \log(L)$. The Z -dependence is less steep than in the Hainich-prescription: $\log(M_{dot}) = \text{const} + 0.42 \times \log(Z)$.

The predictions (observations) in Figures 11 and 12 show very large scatter. A part of this can be due to real differences in clumping parameters (F_{vol} and $FVEL$) which may vary from star to star. This will be discussed in Ch. 6.

5.3. Wind stratifications. Computed wind velocities.

Examples of parameter-stratifications of our solutions are shown in Fig.13 for means of Howarth and Prinja (1989) O-stars and Nugis and Lamers (2000) WR-stars. The differences between O- and WR-stars are due to much larger mass loss rates of WR-stars which reflects in all the parameters shown. Due to the simple modeling one can not expect extremely good fits. In the itera-

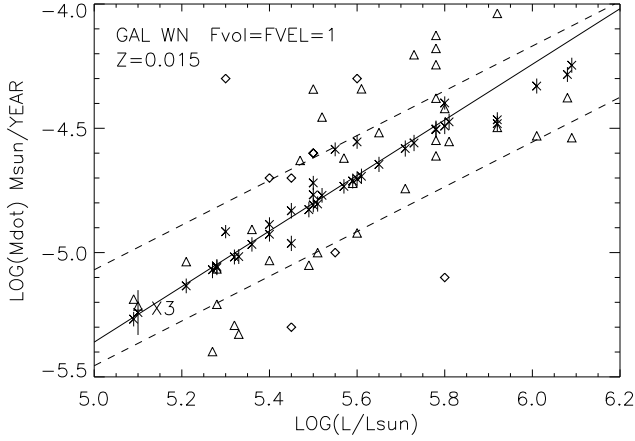


Fig. 11. Mass loss rate vs Luminosity for galactic WN-stars (logarithmic scales, Table A2). Solutions of wind equations for 29 WN-stars from Nugis and Lamers (2000), Cyg X-3 from Vilhu et al. (2009), and 9 hottest Hydrogen-deficient WN-stars from Hamann et al. (2006) are shown with crosses and with (small) error bars (using $Z=0.015$). Both volume and velocity filling factors were set to 1 ($F_{vol} = FVEL = 1$). Triangles show the Nugis and Lamers (+ Cyg X-3) predictions and the solid diagonal line their linear fit. The diamonds show Hamann-predictions. The two dashed lines are Hainich-prescriptions (Hainich et al (2014)) for two heavy element contents $Z = 0.006$ (lower line) and 0.015 (upper line). Cyg X-3 is marked by 'X3'.

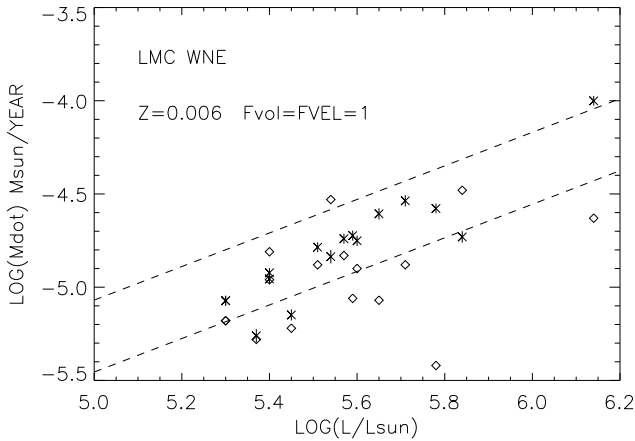


Fig. 12. Mass loss rate vs Luminosity for Large Magellanic Cloud (LMC) WNE-stars (logarithmic scale, Table A2). Solutions of wind equations for 16 Hydrogen deficient hottest stars from Hainich et al (2014) are shown with crosses and with (small) error bars for $Z = 0.006$. Both volume and velocity filling factors were set to 1 ($F_{vol} = FVEL = 1$). The dashed lines are the Hainich-prescriptions for two heavy element contents $Z = 0.006$ (lower) and 0.015 (upper). The diamonds show the observed values of Hainich et al. (2014).

tions chi squares (DOF = 998) for O-stars were ≤ 1 while for WR-stars chi squares ≤ 5 were accepted.

The fitting results are collected in Fig. 14 showing v_{inf} versus the escape velocity v_{esc} . The correlation is rather tight with $v_{inf} = 1.5v_{esc}$. The escape velocity includes the reducing effect of Thomson scattering on gravity by

$$v_{esc} = \sqrt{2GM/R(1 - \Gamma)} \quad (17)$$

where Γ is computed from eq.10 (Kudritzki and Puls (2000), Nugis and Lamers (2000)).

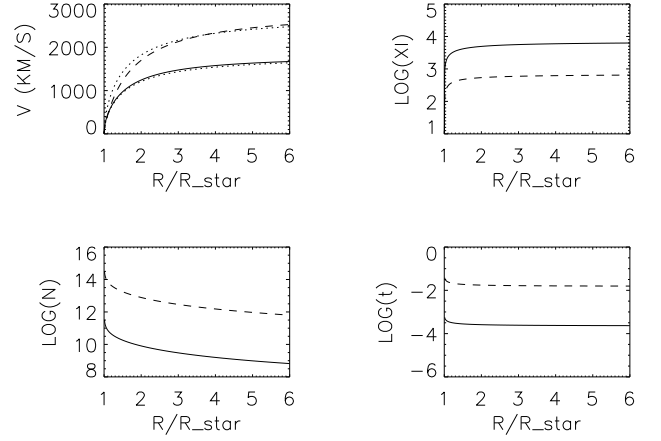


Fig. 13. Fitting results for parameter-stratifications for means of Howarth and Prinja (1989) O-stars in Table A1 (solid lines) and Nugis and Lamers (2000) WR-stars in Table A2 (dashed lines). Upper left: wind velocity vs radial distance. The dotted lines (hardly visible) show the model. Upper right: ionizing parameter $\log(\xi)$ vs radial distance. Lower left: particle number density vs radial distance. Lower right: absorption parameter $\log(t)$ vs radial distance.

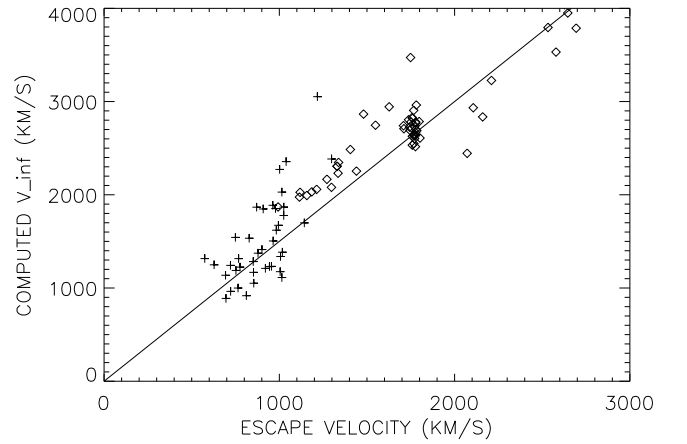


Fig. 14. Computed wind velocities at infinity versus escape velocities for the solutions of program stars (Tables A1 and A2). Pluses: O-stars, open diamonds: WR-stars. The solid line has a slope 1.5.

In principle v_{inf} can be changed, keeping M_{dot} more or less unchanged, by modifying the input parameters β , F_{vol} and $F_{vel} = FVEL$ (see next Chapter). The computed v_{inf} -values for O-stars (Table A1) match with the observed ones given in refs. 1-3 of Table A1. The computed v_{inf} -values for WN-stars (Table A2) are as an average 1.5 times larger than the 'observed' ones given in refs. 4-6 of Table A2 and which scatter around the escape velocities. Using smaller β (instead of 0.6) this difference becomes smaller, v_{inf} is more β -dependent than M_{dot} (see Table 1).

6. Discussion. Effect of parameters.

XSTAR is designed to calculate the ionization and thermal balance in gases exposed to ionizing radiation. It contains a relatively complete collection of relevant atomic processes and corresponding atomic data. It does not, by itself, include processes associated with wind flows, such as shock heating, adiabatic

Table 1. Effect of parameters (β , F_{vol} and $FVEL$) on M_{dot} and v_{inf} for the means of Howarth and Prinja (1989, O-stars) and Nugis and Lamers (2000, WN-stars) samples. Table gives the values by which M_{dot} and v_{inf} should be multiplied if values other than the baseline values ($\beta=0.6$, $F_{vol} = FVEL = 1$) are used, as indicated in the Table.

		$\beta=1$	$F_{vol}=0.1$	$FVEL=0.1$
O-stars	M_{dot}	0.66	4.32	0.02
	v_{inf}	1.42	1.26	1.35
WN-stars	M_{dot}	0.75	1.86	0.08
	v_{inf}	2.70	1.05	0.89

cooling, or time-dependent effects. It also has a simple treatment of radiation transport which provides approximate results in situations involving truly isotropic radiation fields or line blanketing, for example.

When computing the ionization parameter ξ for small filling factors it was assumed that all the mass is in the clumps, without any interclump low density gas with high ionization. This simplified the method but underestimates the ionization if the interclump medium is not empty.

The wind equations included three fixed parameters: F_{vol} , $FVEL$ and β (see eqs 9, 12 and 16). The value 0.13 of F_{vol} for O-stars was selected to fit mass loss solutions with Vink-prediction (Vink et al. 2001) (in addition $FVEL = 0.1$ for weak wind stars, see Section 5.1). For WR-stars it was sufficient to select $F_{vol} = FVEL = 1$ to match the computed mass loss rates with the Hainich-prescriptions (Hainich et al. 2014) and with Nugis and Lamers (2001) predictions. Computed v_{inf} -values of O-stars are similar to the observed ones while for WN-stars the 'observed' values are by a factor 1.5 smaller than the computed ones in Table A2 (see Ch. 5.3).

As an example, the computed mass loss rate of Cyg X-3 is very close to that found from orbital period change $P/P_{dot} = 850000$ y (Kitamoto et al. 1995, Ergma and Yungelson 1998). The observed v_{inf} of Cyg X-3 is uncertain but Vilhu et al. (2009) give for the Si XIV emission line (arising in the photoionized wind) FWHM = 1850 ± 200 km/s and for the P Cygni absorption component at -900 km/s FWHM = 750 ± 200 km/s. These values point to large maximum velocity but somewhat smaller than the computed one given in Table A2 (2533 ± 205 km/s). The X-rays from the compact star may influence these values (to be studied later). If the X-ray suppression on the face-on side in Cyg X-3 is significant it may act in a similar way as lowering FVEL (see Table 1). The mass loss rate will be smaller but this may be compensated by lower wind velocity because the accretion is very sensitive on the wind velocity.

To obtain a quantitative estimate of the influence of these parameters we computed the values by which M_{dot} and v_{inf} should be multiplied if values other than the baseline ones ($\beta = 0.6$, $F_{vol} = FVEL = 1$) are used. These are given in Table 1. The values are given for the means of O-star and WR-star samples. Lowering of F_{vol} or $FVEL$ increases or decreases M_{dot} , respectively. Increasing of β changes M_{dot} and v_{inf} but in opposite way. In particular in WR-stars v_{inf} is sensitive on β .

The velocity clumping parameter $FVEL$ is related to velocity-gradients. Numerical simulations show that after a local velocity jump there follows a region with smaller velocity gradient producing density clumps (Sundqvist et al. 2010). In the smooth wind case (with monotonic velocity law) $\delta v_{sm}/\Delta v$ = clump size /clump separation = $\delta r_{sm}/\Delta r$. Assuming spherical clumps the volume filling factor is by definition $F_{vol} =$

$4/3\pi(\delta r/2)^3/\Delta r^3$. Using this, F_{vel} can be rewritten from eq. 11 as

$$F_{vel} = FVEL = span \times 1.24 F_{vol}^{1/3} / (1 + span \times 1.24 F_{vol}^{1/3}) \quad (18)$$

Here $span = \delta v/\delta v_{sm}$ = velocity span in clumps relative to the smooth wind case. Hence, for the best fit with Vink-prediction of O-stars ($F_{vol} = 0.13$), $FVEL = 0.38$ and 0.98 if the span is 1 and 100, respectively. This may be one area when discussing why low luminosity weak wind stars could have small $FVEL$ -values: sudden change in the wind vorosity when moving from O-type giants towards main sequence.

7. Conclusions

Past work has demonstrated that the CAK-method is successful for giants and supergiants of normal OB-stars but failed to explain the weak winds of main sequence low luminosity OB-stars ('weak wind problem'). Further, CAK was never applied seriously to WR-stars due to the 'momentum problem'. In the present paper the CAK-method has been tested in this context by recalculating force multipliers and integrating the wind equations for a sample of O- and WR stars. Mass loss rates and wind velocities comparable with the observed ones were obtained and as a byproduct solutions for the momentum and weak wind problems suggested.

The work reported in this paper represents a comprehensive effort to model the winds of a large sample of hot stars. It also includes the effects of ionization on the force multiplier computed locally in the wind. Starting from the basic stellar parameters (mass, radius, luminosity, chemical composition) the wind equations were solved in the supersonic part and fitted with the velocity β -law with $\beta=0.6$ (eq. 12) and $v_{in} = 10$ km/s, giving mass loss rates (M_{dot}) and wind velocities (v_{inf}) as the results. These equations included both density and velocity clumpings (F_{vol} and $FVEL=F_{vel}$). The β -law used has no physical justification for WR-stars, neither fixed $\beta=0.6$. However, this was used to show that the wind-acceleration works. Besides the basic stellar parameters the mass loss rate depends also on the velocity law and the subsonic part boundary condition. These were approximated by the values of β and v_{in} .

The results are given in Tables A1 and A2 and Figures 8-12. The resulting mass loss rates were compared with observations/predictions. O-stars require moderate density clumping ($F_{vol} = 0.13$, $FVEL = 1$) when compared with Vink et al. (2001) predictions. WR-winds can be modelled with $F_{vol} = FVEL = 1$. The results depend somewhat on the velocity model used (value of β in eq. 9), for M_{dot} the β -dependence is weaker than for v_{inf} (see Table 3).

The line force multiplier (radiative force) was computed with the XSTAR code and atomic data base as a function of local parameters t (Sobolev line absorption), ξ (ionization parameter) and N (particle number density). The ionizing source (the stellar spectrum) was flexibly specified ranging from blackbodies to realistic computed spectra. It was demonstrated that blackbodies can be used as radiators for O-stars while for WR-stars one should use cut blackbodies (fluxes cut to zero below 230 Å, the He⁺ ionization limit).

The flux below 230 Å is crucial for the size of force multiplier. That part of radiation flux (soft X-rays) can effectively suppress the radiative force. The lack of it in WR-stars, due to the strong absorption in this spectral region, increases the number of lines contributing to the line force and avoids the X-ray suppression (see Figs 2-5). This makes possible to accelerate their massive winds and solves the momentum and single scattering

limit problems. Hence, the 'momentum problem' is an opacity problem as suggested by Gayley et al. (1995).

A possible solution for the 'weak wind problem' of low luminosity late O-stars was quantitatively studied. A small velocity filling factor $FVEL = 0.1$ solves the problem but the physical reason behind this remains to be clarified. As discussed in the previous Chapter the *clumpspan* (velocity span inside a clump relative to the smooth wind case) may be different in giants and main sequence O-stars.

Acknowledgements.

References

- Abbott D.C. 1982, ApJ 259, 282.
- Asplund M., Grevesse N., Sauval A.J. & Scott P. 2009, Ann. Rev. Astron. Astrophys. vol 47, 481.
- Breysacher J., Azzopardi M. & Testar G. 1999, A&AS, 137,117.
- Castor J.I., Abbott D.C. & Klein R.I. 1975, ApJ 195, 157. (CAK).
- Crowther P.A. 2007, Ann.Rev.Astron.Astrophys. vol 45, 177.
- Ergma E. & Yungelson L.R. 1998, A&A 333, 151.
- Gayley K.G., Owocki S.P. & Cranmer S.R. 1995, ApJ 442, 296.
- Hainich R., Ruhling U., Todt H., Oskinova L.M., Liermann A., Gräfener G., Foellmi C., Schnurr O. & Hamann W.-R. 2014, A&A 565, A27.
- Hainich R., Pasemann D., Todt H., Shenar T., Sander A. & Hamann W.-R. 2015, A&A 581, A21.
- Hainich R., Ramachandran V., Shenar T., Sander A.A.C., Todt H., Gruner D., Oskinova L.M. & Hamann W.-R. 2019, A&A 621, A85.
- Hamann W.-R., Gräfener G. & Liermann A. 2006, A&A 457, 1015.
- Howarth I.D. & Prinja R.K. 1989, ApJ Suppl 69, 527.
- Kallman T.R. & Bautista M. 2000, BAAS vol. 32, 1227.
- Kallman T.R. 2018, XSTAR.A Spectral Analysis Tool, version 2.5. NASA, Goddard Space Flight Center, December 14, 2018..
- Kitamoto S., Hirano A., Kawashima K., Miyamoto S., Nagase F., White N., Smale A., Soong Y., Matsuoka M., Kawori N. & Yoshida A. 1995, PASJ 47, 233.
- Krticka J. & Kubat J. 2017, A&A 606,A31.
- Kudritzki R.-P. Puls J. 2000, Ann.Rev.Astr.Astrophys. 38, 613K.
- Kurucz, R.L. 1979, ApJ Suppl. 40, 1-340.
- Marcolino W.L.F., Bouret J.-C., Martins F., Hillier D.J., Lanz T. & Escolano C. 2009, A&A 498, 837.
- Mewe R. & Schrijver J. 1978, A&A 65, 99.
- Nugis T. & Lamers H.J.G.L.M. 2000, A&A 360,227.
- Owocki S. 2013, Stellar Winds in 'Planets, Stars and Stellar Systems' Vol.4. Springer Science-Business Media, Dordrecht, p. 735.
- Owocki S. 2014, astro-ph 1409.2084v, 7Sep 2014.
- Shenar T., Oskinova L.M., Järvinen S.P., Luckas P., Hainch R., Todt H., Hubrig S., Sander A.A.C., Ilyin I. & Hamann W.-R. 2017, A&A 606, A91.
- Stevens I.R. & Kallman T.R. 1990, ApJ 365, 321.
- Sundqvist J.O., Puls J. & Feldmeier A. 2010, A&A 510, A11.
- Sundqvist J.O., Puls J. & Owocki S.P. 2014, A&A 568, A59.
- Sundqvist J.O., Owocki S.P. & Puls J. 2018, A&A 611, A17.
- Todt H., Sander A., Hainich R., Hamann W.-R., Quade M. & Shenar T. 2015, A&A 579, A75.
- van der Hucht K.A., Conti P.S., Lundstrom I. & Stenholm B. 1981, Space Sci. Rev. 28, 227.
- van der Hucht K.A. 2001, New Astron. Rev. 45, 135.
- Vilhu O., Hakala P., Hannikainen D.C., McCollough M. & Koljonen K. 2009, A&A 501, 569S.
- Vink J.S. 2000, Thesis, University of Utrecht.
- Vink J.S., Koter A., & Lamers H.J.G.I.M. 2001, A&A 369, 574.

Table A.1. Basic parameters for O-stars with the results of numerical iterations. Mass M , radius R and luminosity L are in solar units. The computed mass loss rate (\dot{M}) is in solar masses/year and velocity at infinity (V_{∞}) in km/s. The errors (+/-) are formal 1-sigma errors. Solar abundances were used. $F_{vol} = 0.13$ and $FVEL=1$ except for main sequence stars of ref 3 $FVEL=0.1$. For ref 1 and 3 the NAME is HD- or BD-number or the name of the target, or ref 3 it is the model number. chi2 is the chisquare of the fitting (between velocity and model velocity), DOF=998.

NAME	M	R	Log(L)	Log(\dot{M})	V_{∞}	chi2	ref
108	61.0	16.1	5.80	-5.55+- 0.22	1867+- 886	0.6	1
15137	29.0	15.4	5.30	-6.20+- 0.22	1315+- 185	0.2	1
34656	32.0	10.5	5.20	-6.50+- 0.05	1175+- 160	2.5	1
37468	25.0	8.6	4.90	-7.30+- 0.07	1337+- 372	1.5	1
46202	24.0	8.1	4.90	-7.19+- 0.05	1112+- 162	2.5	1
54662	45.0	12.8	5.60	-5.87+- 0.16	2028+- 646	0.5	1
66811	74.0	18.9	6.00	-5.18+- 0.04	1620+-1005	0.8	1
90273	31.0	6.4	5.00	-6.96+- 0.05	2383+- 853	2.2	1
93843	57.0	14.3	5.80	-5.57+- 0.09	2355+-1107	1.2	1
101131	56.0	15.0	5.80	-5.59+- 0.24	2271+-1004	0.4	1
11278.	26.0	11.9	5.10	-6.68+- 0.17	1168+- 162	0.4	1
148937	52.0	15.5	5.70	-5.66+- 0.06	1852+- 489	0.8	1
152247	32.0	17.3	5.40	-6.39+- 0.43	1542+- 704	3.2	1
153919	69.0	23.8	6.00	-5.07+- 0.24	1534+- 789	0.3	1
164492	34.0	12.9	5.40	-6.05+- 0.15	1412+- 330	0.7	1
168076	73.0	13.4	5.90	-5.65+- 0.11	3052+- 795	7.3	1
190864	44.0	13.8	5.60	-5.85+- 0.24	1887+- 682	0.4	1
203064	37.0	14.5	5.50	-6.08+- 0.40	1867+- 861	0.4	1
218195	28.0	12.6	5.20	-6.50+- 0.22	1283+- 243	0.4	1
592603	34.0	8.7	5.20	-6.59+- 0.15	1698+- 576	1.2	1
3255	16.4	7.4	4.74	-7.48+- 0.21	1373+- 574	0.5	2
3505	20.9	8.3	4.97	-6.84+- 0.12	1210+- 266	1.1	2
3755	26.8	9.3	5.19	-6.46+- 0.15	1504+- 407	0.8	2
4005	34.6	10.7	5.42	-6.07+- 0.12	1672+- 514	0.8	2
4255	45.0	12.2	5.64	-5.74+- 0.09	1778+- 616	1.2	2
3253	22.8	13.3	5.25	-6.10+- 0.18	1242+- 210	0.5	2
3503	27.2	13.8	5.41	-5.81+- 0.09	1188+- 296	1.0	2
3753	32.5	14.4	5.57	-5.58+- 0.13	1224+- 494	0.6	2
4003	39.2	14.9	5.71	-5.37+- 0.05	917+- 420	0.6	2
3001	28.8	22.3	5.56	-5.53+- 0.09	1315+- 259	1.3	2
3251	34.0	21.3	5.66	-5.36+- 0.09	1248+- 288	1.2	2
3501	40.4	20.4	5.75	-5.23+- 0.07	1136+- 363	0.8	2
3751	48.3	19.7	5.84	-5.12+- 0.06	999+- 275	0.6	2
4001	58.1	19.0	5.92	-5.12+- 0.07	1051+- 486	0.5	2
4251	70.3	18.4	6.00	-5.15+- 0.07	1231+- 690	1.7	2
216898	17.0	6.7	4.73	-9.20+- 0.09	1229+- 542	1.0	3
326329	19.0	8.1	4.74	-9.29+- 0.04	1847+- 596	2.1	3
66788	26.0	8.7	4.96	-8.95+- 0.13	1384+- 716	0.8	3
ZetaOph	13.0	8.8	4.86	-8.91+- 0.21	888+- 368	0.5	3
216532	12.0	7.6	4.79	-8.93+- 0.18	964+- 329	0.5	3

References. (1) Howarth & Prinja (1989); (2) Krticka & Kubat (2017); (3) Marcolino et al. (2009)

Appendix A: Targets

Table A.2. Basic parameters for WN-stars with the results of numerical iterations. Mass M , radius R and luminosity L are in solar units. The computed mass loss rate (\dot{M}) is in solar masses/year and velocity at infinity (V_{∞}) in km/s. The errors (+/-) are formal 1-sigma errors. Hydrogen deficient abundances were used and for LMC WN-stars (ref. 6) one third of the Galactic heavy element content was adopted. $F_{vol} = FVEL=1$. χ^2 is the chisquare of the fitting (between velocity and model velocity), $DOF=998$. For ref 4 the NAME is the WR-number in the Sixth catalogue of WR-stars (van der Hucht et al. 1981), for ref 5 the WR-number in the Seventh catalogue of WR-stars (van de Hucht 2001) and for ref 6 the BAT99-number (Breysacher et al. 1999).

NAME	M	R	$\text{Log}(L)$	$\text{Log}(\dot{M})$	V_{∞}	χ^2	ref
2	10.0	0.9	5.27	-5.07+- 0.03	3472+- 903	3.2	4
127	10.8	0.9	5.33	-5.02+- 0.03	2785+- 423	4.9	4
1	15.2	1.1	5.57	-4.73+- 0.03	2962+- 551	4.3	4
6	15.6	1.1	5.59	-4.71+- 0.03	2781+- 418	5.0	4
31	10.1	0.9	5.28	-5.06+- 0.03	2692+- 393	5.0	4
51	10.2	0.9	5.28	-5.06+- 0.03	2627+- 335	5.4	4
151	18.5	1.2	5.71	-4.58+- 0.03	2651+- 358	5.5	4
10	10.8	0.9	5.32	-5.02+- 0.03	2643+- 335	5.4	4
21	12.0	1.0	5.40	-4.93+- 0.03	2729+- 389	5.0	4
97	11.3	0.9	5.36	-4.97+- 0.03	2819+- 475	4.6	4
133	8.0	0.7	5.09	-5.27+- 0.03	2725+- 416	5.1	4
138	13.9	1.0	5.51	-4.80+- 0.03	2603+- 300	5.7	4
139	9.3	0.8	5.21	-5.13+- 0.03	2780+- 469	4.8	4
141	15.8	1.1	5.60	-4.70+- 0.03	2635+- 322	5.7	4
157	13.5	1.0	5.49	-4.83+- 0.03	2549+- 265	5.9	4
24	48.0	1.8	6.01	-4.33+- 0.03	3794+- 456	5.3	4
25	57.0	2.0	6.09	-4.25+- 0.03	4040+- 540	5.0	4
47	40.0	1.4	5.92	-4.48+- 0.03	3950+- 523	4.9	4
67	16.1	1.1	5.61	-4.69+- 0.03	2688+- 352	5.5	4
115	13.6	1.0	5.50	-4.81+- 0.03	2828+- 480	4.6	4
136	19.1	1.2	5.73	-4.56+- 0.03	2700+- 391	5.3	4
153	14.0	1.1	5.52	-4.77+- 0.03	2741+- 449	4.7	4
155	17.0	1.2	5.65	-4.65+- 0.03	2770+- 408	5.1	4
22	55.3	1.9	6.08	-4.28+- 0.03	3787+- 293	5.9	4
78	21.5	1.3	5.80	-4.49+- 0.03	2608+- 300	5.8	4
87	40.0	1.5	5.92	-4.47+- 0.03	3530+- 249	6.2	4
40	20.6	1.3	5.78	-4.50+- 0.03	2635+- 355	5.5	4
147	20.6	1.3	5.78	-4.51+- 0.03	2668+- 371	5.4	4
105	21.8	1.3	5.81	-4.47+- 0.03	2516+- 254	6.1	4
Cyg X-3	10.0	1.0	5.10	-5.24+- 0.03	2533+- 205	6.0	7
1	15.0	1.3	5.40	-4.89+- 0.03	2905+- 500	4.6	5
2	16.0	0.9	5.45	-4.96+- 0.03	3226+- 389	5.5	5
6	19.0	2.6	5.60	-4.55+- 0.03	2347+- 464	3.7	5
7	16.0	1.4	5.45	-4.83+- 0.03	2716+- 411	5.0	5
18	17.0	1.5	5.50	-4.77+- 0.03	2804+- 449	4.6	5
37	17.0	1.9	5.50	-4.72+- 0.03	2746+- 592	3.6	5
46	25.0	2.1	5.80	-4.40+- 0.03	2943+- 660	3.7	5
36	13.0	1.9	5.30	-4.92+- 0.03	2485+- 537	3.6	5
44	18.0	3.1	5.55	-4.58+- 0.03	2057+- 376	3.7	5
1	12.0	1.9	5.30	-5.07+- 0.03	2306+- 471	4.0	6
2	13.0	0.8	5.37	-5.26+- 0.04	2444+- 279	7.7	6
3	16.0	3.0	5.51	-4.79+- 0.03	1992+- 441	3.2	6
5	15.0	0.9	5.45	-5.15+- 0.03	2933+- 260	5.2	6
7	25.0	1.1	5.84	-4.73+- 0.03	2835+- 391	5.3	6
15	17.0	2.6	5.57	-4.74+- 0.03	2165+- 419	3.6	6
19	39.0	6.3	6.14	-4.00+- 0.03	1869+- 524	2.9	6
24	17.0	2.0	5.54	-4.84+- 0.04	2865+- 701	3.2	6
36	21.0	3.8	5.71	-4.54+- 0.03	2026+- 442	3.0	6
37	19.0	3.6	5.65	-4.61+- 0.03	1975+- 461	3.0	6
41	18.0	2.1	5.60	-4.75+- 0.03	2254+- 281	4.5	6
47	18.0	2.6	5.59	-4.72+- 0.03	2080+- 320	4.1	6
48	14.0	2.1	5.40	-4.96+- 0.03	2231+- 489	4.0	6
51	12.0	1.9	5.30	-5.07+- 0.03	2306+- 471	4.0	6
57	14.0	2.7	5.40	-4.92+- 0.03	2031+- 492	3.4	6
66	35.0	3.3	5.78	-4.58+- 0.03	2708+- 399	4.8	6

References. (4) Nugis & Lamers (2000); (5) Hamann et al. (2006); (6) Hainich et al. (2014); (7) Cyg X-3 Vilhu (2009)